Atmospheric Research 282 (2023) 106532

Contents lists available at ScienceDirect

Atmospheric Research

journal homepage: www.elsevier.com/locate/atmosres

Alternate modulations of ENSO and the Arctic Oscillation on winter extreme cold events in China

Weiwei Wang [a], Song Yang [a,b], Qingquan Li [c], Tuantuan Zhang [a,b,*], Xingwen Jiang [d]

[a] School of Atmospheric Sciences, Sun Yat-sen University; Southern Marine Science and Engineering Guangdong Laboratory (Zhuhai), Zhuhai 519082, China
[b] Guangdong Province Key Laboratory for Climate Change and Natural Disaster Studies, Sun Yat-sen University, Zhuhai 519082, China
[c] National Climate Center, China Meteorological Administration, Beijing 100081, China
[d] Institute of Plateau Meteorology, China Meteorological Administration, Chengdu, Sichuan 610072, China

ARTICLE INFO

Keywords:
Cold events
ENSO
The Arctic Oscillation
Interdecadal shift

ABSTRACT

Station observations and global reanalysis datasets were applied to investigate the dominant modes of winter cold days (CDs) in China and their relationships with the Arctic Oscillation (AO) and El Niño–Southern Oscillation (ENSO). The dominant modes of the CDs exhibited an interdecadal shift around the 1980s. The first mode reflected a nearly coherent interannual variability with a maximum center over central-northeastern China during 1961–1985 (P1), whereas the maximum center shifted to central-southwestern China during 1993–2017 (P2). The second mode represented a north-south dipole variation, with maximum variations over southern China in the P1 but northeastern China in the P2. The first mode was significantly related to the AO in the P1 and ENSO in the P2, whereas the second mode was closely linked to ENSO in the P1 and the AO in the P2. During the P1, an anomalous quasi-barotropic cyclone over northern East Asia was induced by a negative AO, deepening the East Asian trough along the East Asian coast, which was favorable for the occurrence of CDs over central-northeastern China (i.e., the first mode). The El Niño excited an anomalous anticyclonic circulation over the Northwest Pacific, impeding cold air along the coast of southern China, which seemed to produce a pattern of the second mode. During the P2, the AO was weaker (smaller magnitude), and the AO-related anomalous cyclone shifted northwestward compared to that in the P1, limiting its effect to northeastern China and inducing a north-south dipole pattern. On the other hand, ENSO-related anomalous circulation shifted southwestward compared to the P1, modulating CDs over central-southwestern China and producing an anomalous pattern of CDs similar to the first mode.

1. Introduction

Extreme cold events exert devastating effects on human health, economic development, and regional ecosystems (McMichael, 2013; Curtis et al., 2017; Shang and Zhang, 2021). As one of the hardest hit area, China has experienced several mega extreme cold events (Wen et al., 2009; Wang and Chen, 2010; Wang et al., 2021), for example, the long-lasting snowstorms in January 2008 (Wen et al., 2009; Zhou et al., 2009; Wang et al., 2020), the extreme cold temperatures in January 2016 (Song and Wu, 2017) and from late December 2020 to mid-January 2021 (Zhang et al., 2021). During the boreal winter of 2020/21, successive extreme cold events occurred over China. Specifically, cold air outbroke swept across East Asia from Siberia in late December 2020, causing record-breaking cold surface air temperatures and freezing-related damages (Yang and Fan, 2022). Extremely cold temperatures reached −19.6 °C and −19.9 °C in Beijing and Tianjin respectively on 7 January 2021, breaking their previous coldest record on the same date in 1967 (Zhang et al., 2021). A deeper understanding of winter extreme cold events and associated mechanisms is critical for socioeconomic planning in China.

The spatial-temporal characteristics of extreme cold events in China have been investigated by several studies (e.g., Kang et al., 2009; Chen et al., 2013a; Shi et al., 2018; Gao et al., 2021; Zuo et al., 2021). There are remarkable interannual variations of winter surface air temperature over China, of which the two dominate modes are depicted by a spatially consistent pattern and a north-south dipole pattern (Kang et al., 2009;

* Corresponding author at: School of Atmospheric Sciences, Sun Yat-sen University; Southern Marine Science and Engineering Guangdong Laboratory (Zhuhai), Zhuhai, Guangdong 519082, China.
E-mail address: zhangtt75@mail.sysu.edu.cn (T. Zhang).

https://doi.org/10.1016/j.atmosres.2022.106532
Received 6 July 2022; Received in revised form 23 October 2022; Accepted 18 November 2022
Available online 22 November 2022

Xiao et al., 2018; Zuo et al., 2021). Similarly, the first mode of winter extreme cold events also showed consistent spatial variability (Fu and Ding, 2021).

The extreme cold events also exhibit remarkable interdecadal changes in China. While the winter temperature in China showed an overall upward trend during the past six decades, it remained stable after 2006 and the extreme cold events increased apparently (Cui et al., 2017; Fu and Ding, 2021). On the other hand, several studies have demonstrated that the number of winter extreme cold days (CDs) experienced a significant decrease after the mid-1980s with a decline rate of 0.5–4.5% (−3.9 days) per decade in almost the entire country (Chen et al., 2013a; Zhou et al., 2016; Shi et al., 2018; Gao et al., 2021; Zhao and Chen, 2021). However, Cheung et al. (2015) found that the number of CDs in Hong Kong appeared to increase from the late 1990s to the 2000s. Apparently, there is disagreement in terms of the interdecadal changes in extreme cold events, which warrants further investigations.

Substantial efforts have been dedicated to identify the physical causes responsible for the interannual-interdecadal variability of extreme cold events (Park et al., 2011; Chen et al., 2013a; Chen et al., 2013b; Jian et al., 2021). The East Asian winter monsoon (EAWM) is one of the main factors for the extreme cold events in East Asia, on both interannual and interdecadal time scales (Cheung et al., 2015; Hu et al., 2015; Wang and Lu, 2017). More extreme cold events tend to occur when the EAWM is strong, whereas when the EAWM is weak, cold events occur less frequently in East Asia (Wang et al., 2009; Wang and Chen, 2013; Zuo et al., 2021). In addition, it is also reported that the Arctic Oscillation (AO) and El Niño–Southern Oscillation (ENSO) could significantly modulate the interannual variability of cold surges over East Asia (Park et al., 2011; Chen et al., 2013a; Lu et al., 2016; Lu and Zhou, 2018; Song and Yan, 2021). Negative AO and La Niña are favorable for the occurrence of cold surges (He et al., 2017; Zheng et al., 2021). These relationships of interannual variation of the extreme cold events in China with the AO and ENSO displayed interdecadal changes, as pointed out by previous studies (Cheung et al., 2012; Chen et al., 2013a; Yun et al., 2014; Liu et al., 2017; Jian et al., 2021). For example, Chen et al. (2013a) indicated that a significant connection existed between the winter extreme CDs in eastern China and AO before the mid-1980s, while the extreme CDs in southern China are closely linked to ENSO after the mid-1980s. On the other hand, Jian et al. (2021) found that a significant connection between ENSO and winter synoptic temperature variability over eastern China occurred before the mid-1980s, and this connection became insignificant after 1988. The AO and ENSO play important roles in prediction of the winter extreme cold events, and it is important to consider whether there is a stable relationship between the two systems and the cold events in China. It should be noted that the results may be affected by the definition of cold events. Therefore, the current study will reexamine the spatiotemporal variations of winter CDs in China, and further investigate the relative roles of AO and ENSO in the first two leading modes of the CDs during the different periods.

The rest of this paper is organized as follows. The datasets and methods applied are described in Section 2. The spatiotemporal characteristics of China extreme cold events, including the interdecadal changes in their dominant modes, are displayed Section 3. The interdecadal shift in the relationships of the CDs with the AO and ENSO, and the associated mechanisms, are discussed in Sections 4 and 5. Finally, a summary of the study and further discussions are provided in Section 6.

2. Data and methods

The observational station data of daily minimum temperature (Tmin) of 1964 meteorological stations within mainland China from 1961 to 2018 are used in this study. This dataset is collected from the China National Stations' Fundamental Elements Datasets V3.0 (Ren et al., 2012; Cao et al., 2016). Quality-control procedures have been applied to improve the data quality and integrity (Cao et al., 2016; Deng et al., 2019).

Currently, the fifth generation European Centre for Medium-range Weather Forecasts reanalysis (ERA5) for the global climate and weather is available from 1950, which splits into the Climate Data Store entries for 1950–1978 and from 1979 to update (Hersbach et al., 2020; Bell et al., 2021). Monthly geopotential heights, sea surface temperature (SST), vertical velocity and winds from the ERA5 (accessed from the Copernicus Climate Change Service Climate Data Store) with a horizontal resolution of 1° × 1° are utilized. The monthly AO index and Niño-4 index are obtained from https://www.cpc.ncep.noaa.gov/products/precip/CWlink/daily_ao_index/monthly.ao.index.b50.current.ascii.table and https://www.cpc.ncep.noaa.gov/data/indices/ersst5.nino.mth.91-20.ascii, respectively.

Considering the significant difference in regional climatology, the relative threshold is more meaningful to detect the local extremes in China (Deng et al., 2019; Zhang et al., 2022). In this study, the CDs are defined based on a 10th percentile method, which is widely used in previous studies (e.g., Chen et al., 2013a; Cheung et al., 2015; Grotjahn et al., 2015; Shi et al., 2018; Om et al., 2022). For a specific day in December–January–February (DJF), its threshold is determined by the 10th percentile of Tmin for a total of 870 days (58 × 15; the 15 days correspond to 7 days on either side of the target date) for the 58 years (1961–2018). By moving the 15-day sampling window forward or backward, we can obtain a consecutive threshold for every day. An extreme CD is identified when Tmin is below the threshold. Then, the number of extreme cold events is obtained by the cumulative number of CDs during each winter. In this study, the winter of a specific year is defined as the December of the current year and the January–February of the following year.

In order to extract the dominant modes of China CDs, we apply the Empirical Orthogonal Function (EOF) analysis to the cold events. An area-weighted method is applied at each station by multiplying the square root of the cosine of latitudes (North et al., 1982; Dawson, 2016; Deng et al., 2019). Other analysis methods conducted include linear correlation and linear regression. All data used in this study are detrended before further calculations of correlation and regression to focus on the interannual variations of cold events. The Student's *t*-test and *P*-value are applied to assess the statistical significance of the results obtained.

3. Spatiotemporal characteristics of China extreme cold events during 1961–2017

The climatological CDs and 10th percentile thresholds of Tmin in DJF are presented in Fig. 1a–b for 1961–2017, respectively. The spatial distribution of the 10th percentile threshold shows a north-low–south-high structure (Fig. 1b), which is similar to the climatology of Tmin (figures not shown). Specifically, the threshold exceeding 0 °C appears to the south of 25°N and over the Sichuan Basin. The lowest threshold is below −30 °C over northern China and the highest threshold reaches about 6–8 °C over southern China. On the other hand, the winter CDs in climatology show a relative uniform distribution (about 8–10 days per year) in China during 1961–2017 (Fig. 1a). While the interannual variability of Tmin in China displayed an increasing magnitude after the 1980s, there was a weaker interannual oscillation of China CDs after 1980s (Fig. 1c). The number of winter CDs in China varied from 4 to 24 days during 1961–1985 (P1) and in the range of 0–8 days during 1993–2017 (P2). Apparently, there is less winter CDs after 1985, which could be partly related to the increase in Tmin (Fig. 1c). This interdecadal shift around 1985 was further verified by the 10-year sliding *t-test* (Fig. 1c), and was basically consistent with Chen et al. (2013a).

The dominant modes of detrended winter CDs over China are extracted by EOF and are presented in Fig. 2. The first EOF mode (EOF1) of CDs reflects a coherent interannual variability with a maximum center over central China (Fig. 2a), similar to the pattern of

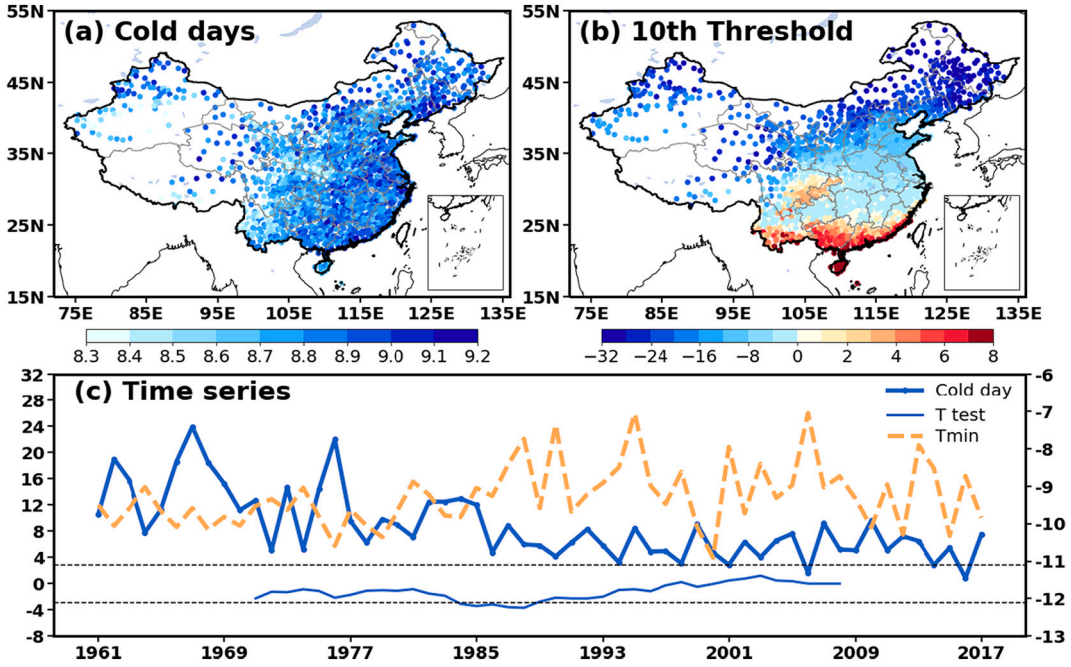

Fig. 1. Maps of (a) CDs and (b) 10th percentile thresholds in boreal winter (DJF) during 1961–2017 from in-situ observations. (c) Time series of China winter CDs (thick blue line) and Tmin (dashed orange line). The thin blue line represents the 10-year sliding *t*-test for the CD series, and the dashed horizontal line denotes the 95% confidence level. (For interpretation of the references to colour in this figure legend, the reader is referred to the web version of this article.)

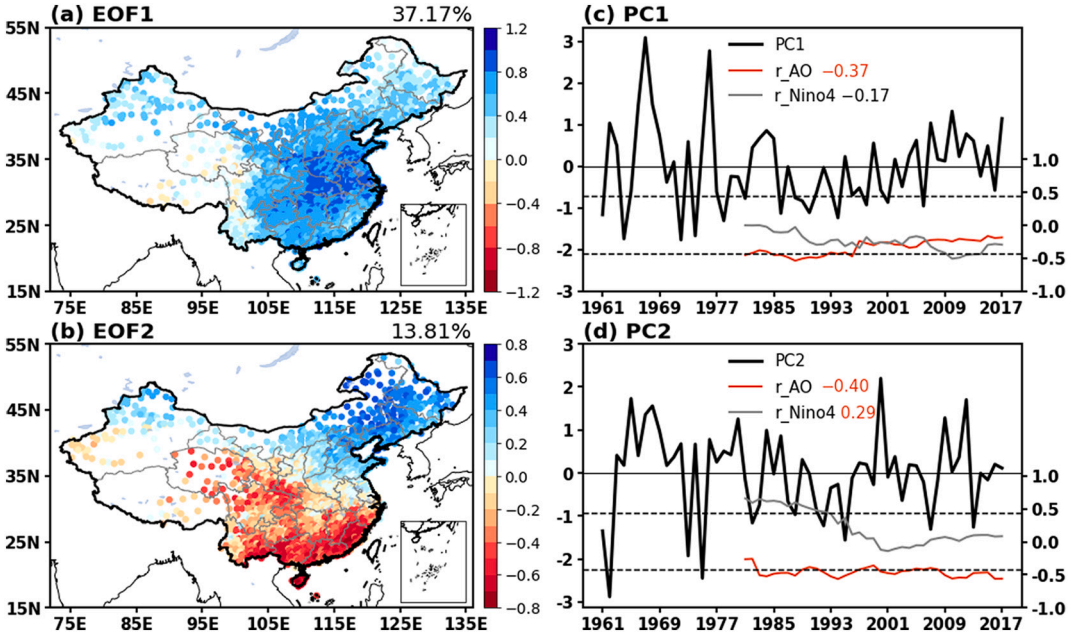

Fig. 2. Spatial patterns of (a) first and (b) second EOF modes of detrended winter CDs over China, and (c–d) the corresponding PCs (black line). In (c-d), the red (grey) line represents the 21-year sliding correlation coefficient between the PCs and the AO (Niño-4) index, and the dashed horizontal line denotes the 95% confidence level. The correlation coefficients of the PCs with the AO and Niño-4 indices during1961–2018 are shown in (c) and (d), with red fonts representing the significant values exceeding the 95% confidence level. (For interpretation of the references to colour in this figure legend, the reader is referred to the web version of this article.)

climatological winter CDs (Fig. 1a). While the second mode (EOF2) is depicted by a north-south dipole structure over China (Fig. 2b). These spatial patterns of dominant modes are consistent with previous studies (Kang et al., 2009; Xiao et al., 2018; Zuo et al., 2021). The EOF1 and EOF2 account for 37.17% and 13.81% of the interannual variability of China cold events, respectively, together explaining more than half of the total variance. These two modes are statistically distinguishable from each other, according to the rule by North et al. (1982). Therefore, we mainly focus on the two leading modes in this study. The corresponding principal component (PC1 hereafter) of EOF1 exhibits a weaker interannual oscillation during the P2 than that during the P1 (Fig. 2c), consistent with the interdecadal shift of the area-averaged CDs of the entire country (Fig. 1c). The correlation coefficient between the PC1 and the CDs averaged over China is 0.996, statistically exceeding

the 99.9% confidence level. On the other hand, there is no apparent interdecadal shift around 1985 for the principal component (PC2 hereafter) of EOF2 (Fig. 2d).

4. Interdecadal shift in the oceanic-atmospheric processes associated with extreme cold events over China

The interannual variation of extreme cold events over China and the associated oceanic-atmospheric processes are investigated separately for the P1 and the P2, regarding to the interdecadal shift of both the national-averaged and the first mode of extreme cold events around 1980s. The climatological winter CDs during the P1 and the P2 from the in-situ observations are presented in Fig. 3a and b, respectively. The number of winter CDs in climatology changes from 9 to 15 days per year in the P1 to 4–7 days per year in the P2 (Fig. 3a–b). Compared with the whole period, the spatial patterns show a relative inhomogeneous feature in the P1 and the P2. During the P1, the largest frequency of CDs around 13–15 days per year is located over central-northeastern China, where the CDs occur less frequently compared to other parts of China during the P2 (Fig. 3a–b).

The first two dominant modes are further presented in Fig. 4. According to the rule by North et al. (1982), the first two leading modes of CDs, which account for above 50% of the total variances during the two periods, are statistically distinguishable from each other. During the P1, the first two modes were respectively depicted by a nearly national-coherent structure and a north-south dipole structure, similar with those during the whole period (Figs. 2a–b and 4a–b). During the P2, the first mode was characterized by positive anomalies over most regions and slightly negative anomalies over northeastern China and the Tibetan Plateau (TP) (Fig. 4c). The largest interannual variation shifted from central-eastern China in the P1 to central-southwestern China in the P2 (Fig. 4a and c). The second mode also represented a north-south dipole variation, but the maximum center was located over northeastern China, instead of over southern China as in the P1 (Fig. 4b and d). The EOF2 accounted for 21.57% of the total variance in the P2, more than that in the P1, suggesting that the north-south dipole variation appeared more frequently in the P2. In addition, the corresponding PCs were presented in the right panels of Fig. 4. The coefficient of correlation between the PC1 and detrended national-averaged winter CDs (Figs. 3c–d) was 0.99 and 0.92 in the P1 and the P2, respectively (Fig. 4e and g), indicating that the first modes well reflected the overall interannual variability of CDs in China.

We further analyze the atmospheric circulations and SST anomalies related to the dominant modes of winter extreme cold events in China. Hereafter, the PC1 and PC2 in the P1 and P2 are briefly denoted as the PC1_P1, PC1_P2, PC2_P1, and PC2_P2, respectively. Fig. 5 presents the regression patterns of geopotential heights, winds, and SST upon the PC1 for the two periods. Corresponding to the positive phase of PC1_P1 during the P1, at the upper and middle levels (200 hPa and 500 hPa), significant positive anomalies of geopotential height occupied the high latitudes, and significant negative geopotential height anomalies and an anomalous cyclonic circulation appeared over central-northern China (Fig. 5a–b). The quasi-barotropic anomalous cyclonic circulation signified a deepening East Asian trough along the East Asian coast (Fig. 5a–b), facilitating the intrusion of cold air from Siberia to China (Park et al., 2011). Correspondingly, at the lower-level (850 hPa), anomalous northerly winds appeared over China (Fig. 5e), favoring the occurrence of extreme cold events over the entire country, in particular for northern China. There were basically insignificant SST anomalies associated with the first mode in the P1 (Fig. 5e). These anomalous atmospheric processes over the mid-higher latitudes were similar to those associated with the negative phase of the AO (Park et al., 2010, 2011; Yang et al., 2020). In the P2 for PC1_P2, at the upper troposphere, an anomalous anticyclonic circulation with positive geopotential height anomalies and an anomalous cyclonic circulation with negative geopotential height anomalies appeared over southern and northern China, respectively (Fig. 5c). The atmospheric anomalies became weaker at the middle-level (Fig. 5d). At the lower-level, there was an anomalous cyclonic circulation over southern China-northwestern Pacific, which induced anomalous northerly winds and favored the occurrence of extreme cold events over southern China (Fig. 5d and f). This lower-level anomalous cyclonic circulation seemed to be associated with a La Niña-like SST pattern in the tropical Pacific (Fig. 5f), and the upper-level anomalous anticyclonic circulation was more likely a response to the

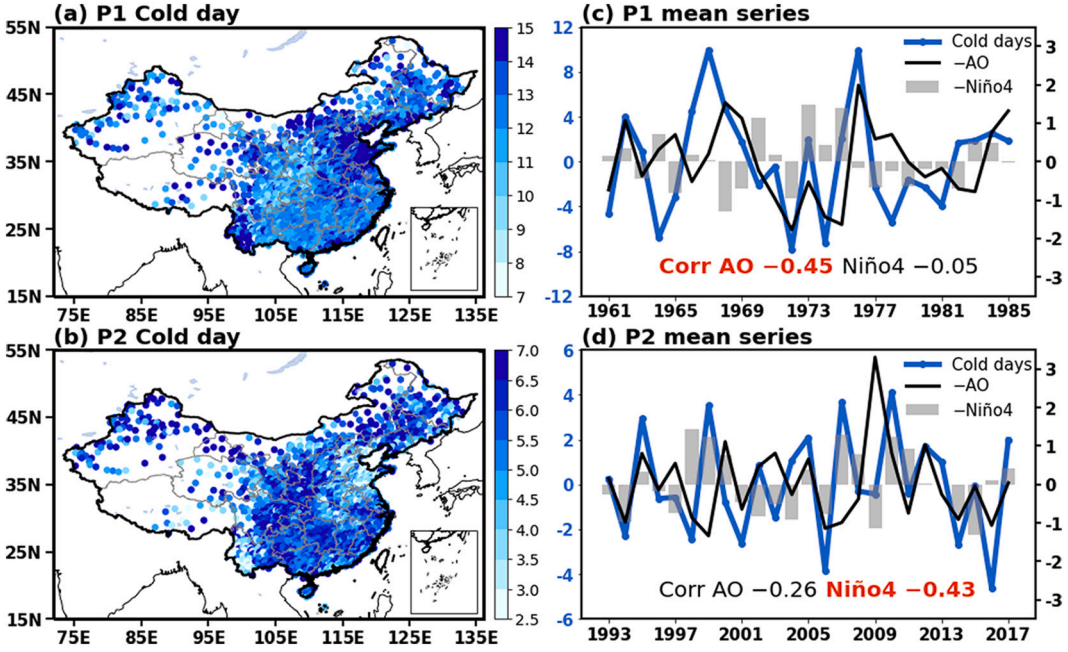

Fig. 3. Maps of winter CDs during the (a) P1 and the (b) P2 from in-situ observations, and (c, d) corresponding detrended time series of China CDs (blue line), AO (black line), and Niño-4 index (grey bar). The correlation coefficients of the CDs with the AO and Niño-4 indices during the P1 and the P2 are shown in (c) and (d), respectively. The red fonts denote the significant values exceeding the 95% confidence level. (For interpretation of the references to colour in this figure legend, the reader is referred to the web version of this article.)

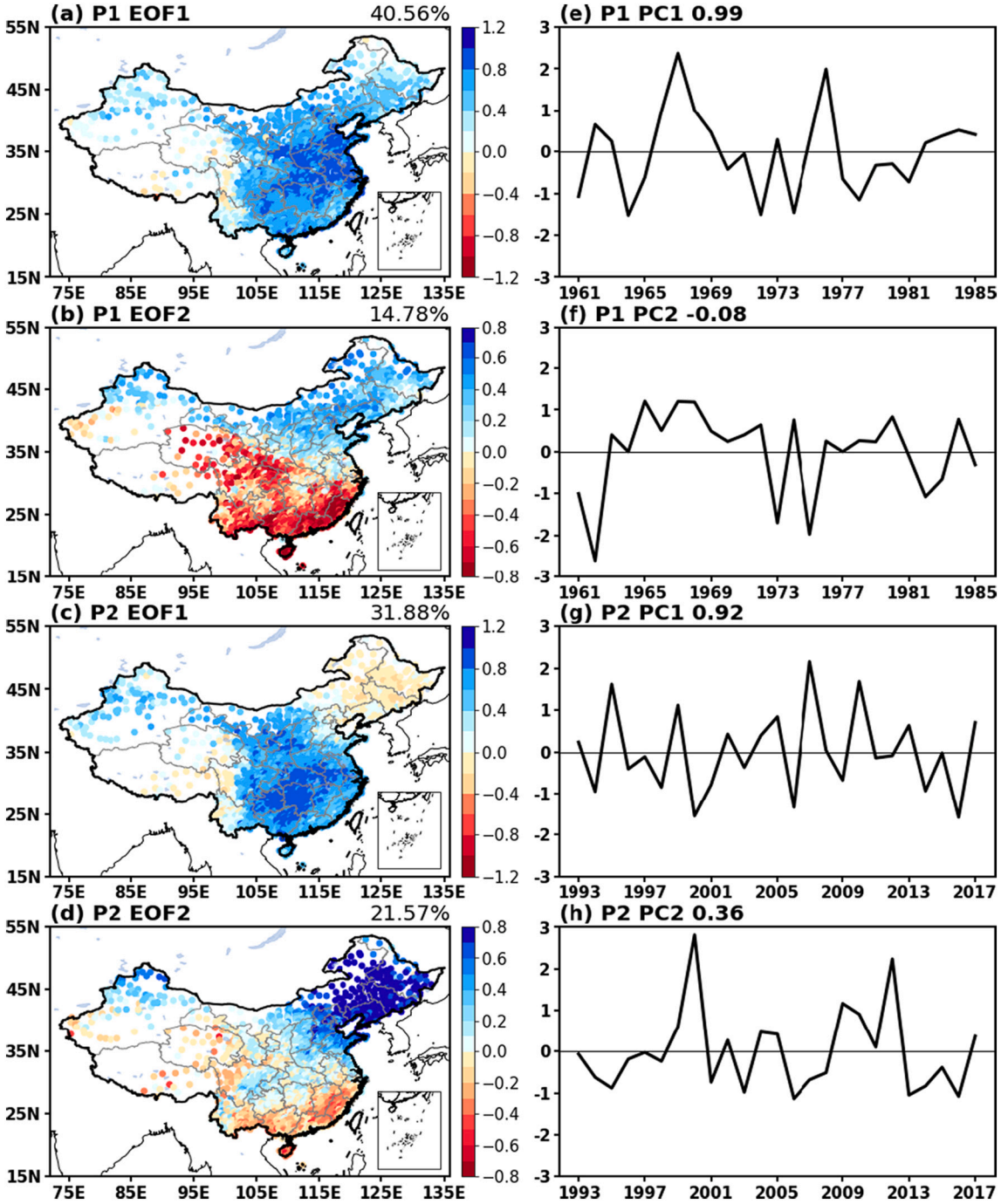

Fig. 4. (a–d) The spatial patterns for the first two EOF modes of detrended winter CDs over China, and (e–h) the corresponding PCs (black line) during the periods of P1 (top four panels) and P2 (bottom four panels). Correlation coefficients between the PCs and the area-averaged CDs in China are presented in the right panels.

low-level heating (modulation on the local Hadley circulation). The anomalous circulations over northeastern China were weaker, consistent with the slight oscillation of CD frequency of EOF1 in northeastern China (Figs. 4c and 5e–f). From the above, the first mode in the P2 might be mainly affected by the low-level circulation, instead of the upper-level processes.

Regression maps of 200-hPa and 500-hPa geopotential height and winds, 850-hPa winds and SST onto the PC2s in the P1 and the P2 are shown in Fig. 6. In the P1 for PC2_P1, the north-more–south-less pattern of CDs was accompanied by upper- and middle-level anomalous anticyclone over southeastern China-northwestern Pacific and anomalous cyclone to its northwest (Fig. 6a). The associated upper- and middle-tropospheric circulation might be regulated remotely by both tropical and extra-tropical systems (Fig. 6a–b). From Fig. 6e, significant warm SST anomalies were observed in the tropical central Pacific (Fig. 6e), suggesting that the equatorial central Pacific is a key region for regulating the CDs in China. There were lower-level anomalous anticyclonic circulations that induced significant anomalous southerlies over southern China, impeding intrusion of the cold air into southern China (Fig. 6e). In contrast, there was weak SST signal for PC2_P2 (Fig. 6f). The lower-level anomalous southerlies were weaker compared to those in the P1 (Fig. 6e–f), consistent with the moderate magnitude of interannual variation of CDs in the P2 (Fig. 4b and d). At the middle and upper levels, there was an anomalous cyclone to the north of 40°N, inducing

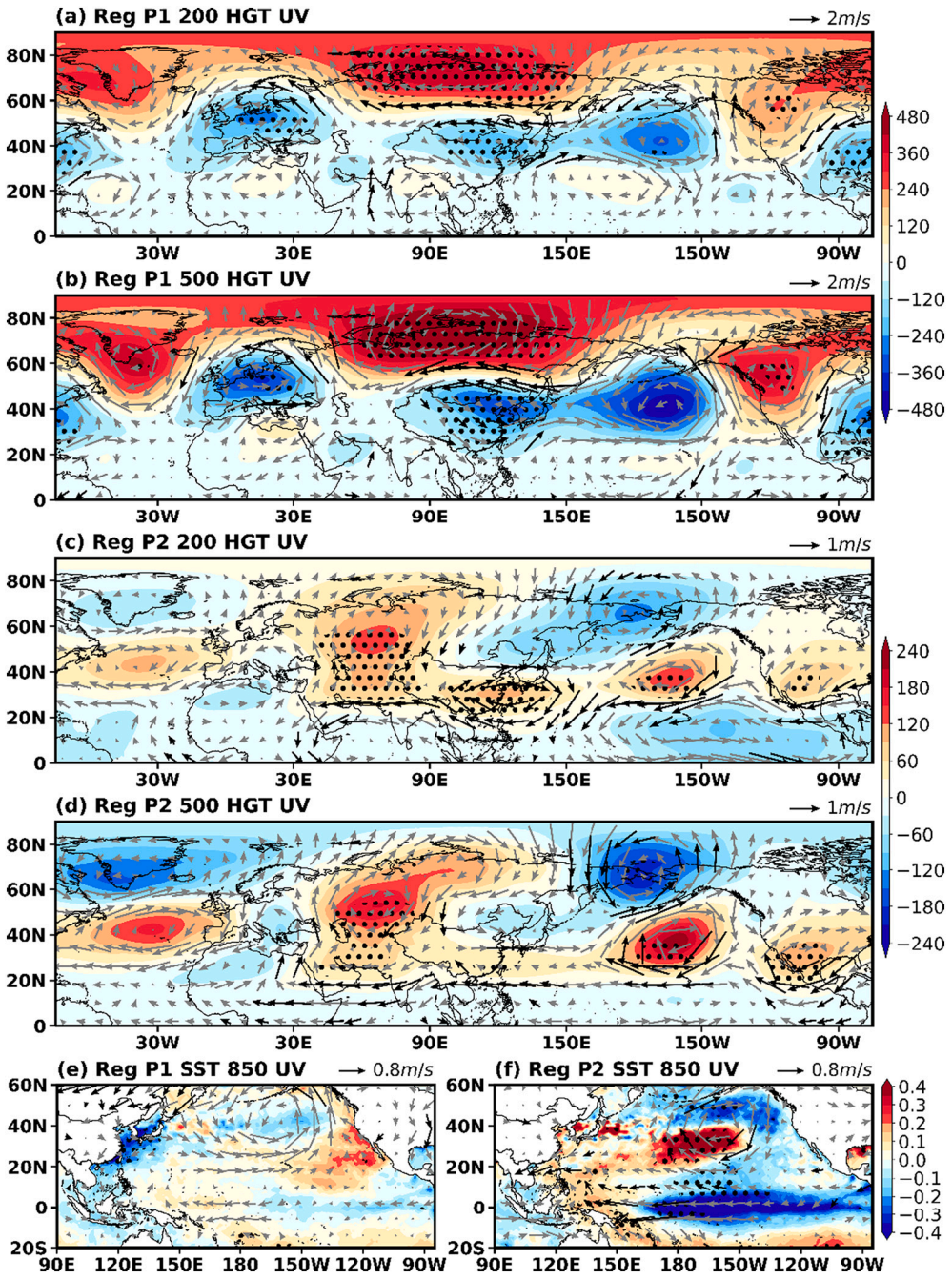

Fig. 5. Regression maps of 200-hPa and 500-hPa geopotential height (shading; Pa) and winds (vectors; m s^{-1}) onto the PC1s for the P1 (a–b) and for the P2 (c–d). (e–f) Same as in (a, c), but for 850-hPa winds (vectors; m s^{-1}) and SST (shaded; °C). Significant values exceeding the 95% confidence level are marked by black dots or vectors.

easterly anomalies and bringing cold air from Siberia to northeastern China (Fig. 6c and d).

5. Relative roles of the AO and ENSO in the two periods

The AO and ENSO play important roles in the interannual variability of climate over East Asia by remotely regulating atmospheric circulations (He et al., 2017; Wang and Lu, 2017). The above analysis suggests that the extreme cold events over China may be affected by the AO and ENSO in different periods. From Fig. 2c–d, the corresponding PCs of the dominant modes during the whole period show distinctive relationships with the AO and ENSO. Both the PC1 and the PC2 are significantly correlated with the AO index during the whole period, with correlation coefficients of −0.37 and −0.40 for PC1 and PC2, respectively. On the other hand, ENSO is insignificantly correlated with the PC1 ($R = -0.17$) but significantly correlated with the PC2 ($R = 0.29$) during the whole period. Apparently, these relationships exhibit inter-decadal changes, and the results varies in the different periods. The PC1-AO relationship was significant only before the 1990s, and after that, the PC1-ENSO relationship became significant (Fig. 2c). The PC2 was basically significantly connected with the AO with an exception for 1961–1982 and is significantly related to ENSO only before the 1990s (Fig. 2d). In fact, the interannual variations of the AO and the CDs averaged over China were consistent during the P1 ($R = -0.45$) (Fig. 3c) but distinctive from each other during the P2 ($R = -0.26$) (Fig. 3d). ENSO displayed an opposite relationship with the CDs averaged over China during the two periods

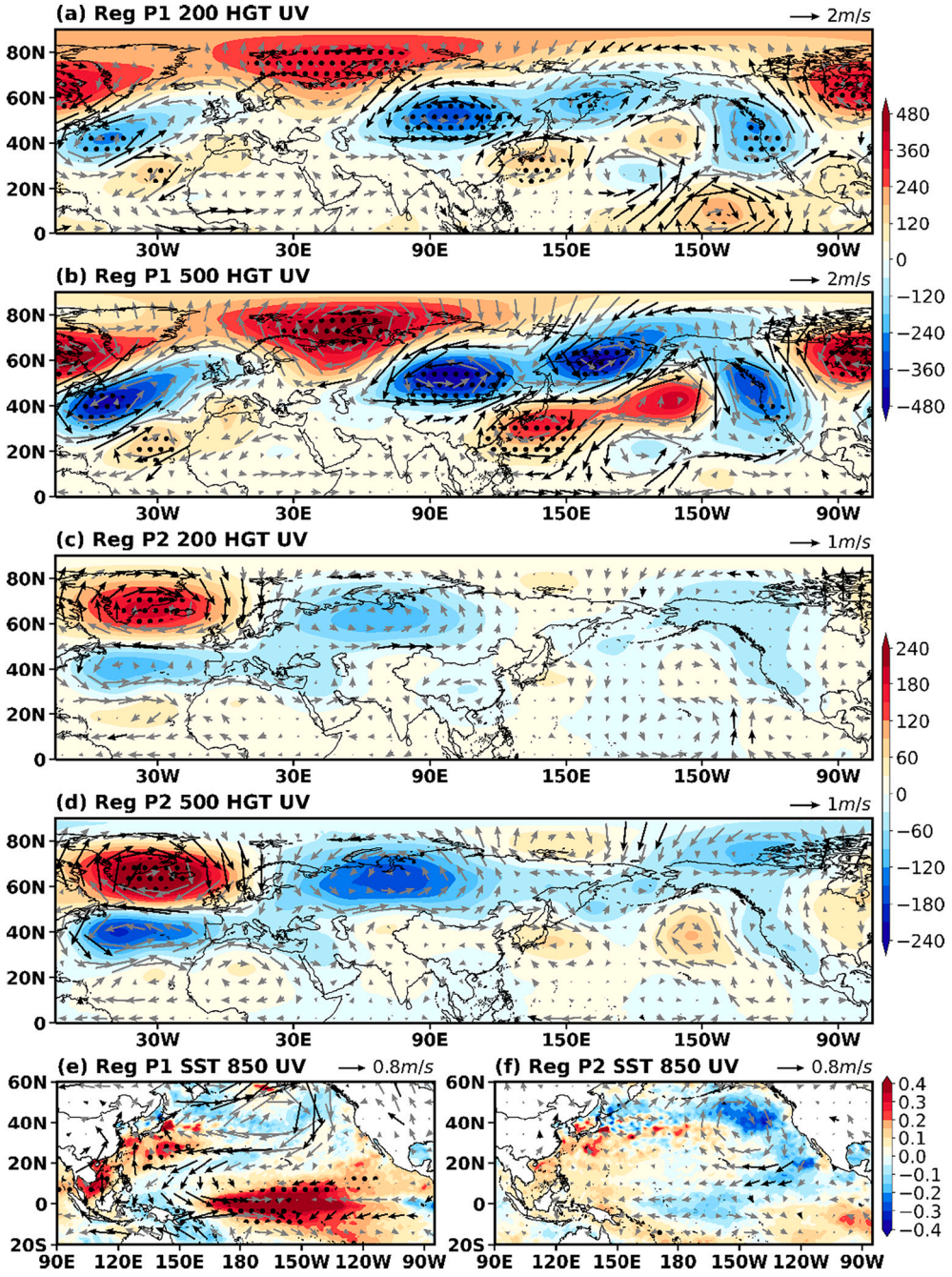

Fig. 6. Same as in Fig. 5, but for the PC2s.

(Fig. 3d). In addition, the relationships between the first two modes of the cold events and the AO and ENSO indices are listed in Table 1. The PC1_P1 showed a significant relationship with the AO ($R = -0.43$) and an insignificant relationship with ENSO ($R = -0.01$) in the P1, whereas PC1_P2 exhibited opposite relationships with the AO ($R = -0.06$) and ENSO ($R = -0.40$) in the P2, similar to the features for the CDs averaged over China. On the other hand, the second mode was significantly connected with ENSO ($R = 0.51$) in the P1 but significantly associated with the AO ($R = -0.55$) in the P2.

Table 1
Correlation coefficients of PC1s and PC2s with the AO index and the Niño-4 index for different periods. Boldface denotes the significant values with correlation coefficients exceeding the 95% confidence level.

Period	Index	PC1	PC2
1961–1985	AO	**−0.43**	−0.18
	Niño4	−0.01	**0.51**
1993–2017	AO	−0.06	**−0.55**
	Niño4	**−0.40**	−0.20

We further investigate how and why the AO and ENSO affect the extreme cold events over China in different periods. As shown in Fig. 7a–b, significant negative correlations between the CDs and the AO index were observed over central-northeastern China in the P1, and a north-south dipole pattern with maximum variation over southern China was found from the correlation maps of CDs with Niño-4 index. These correlation patterns were similar to those associated with the EOF1 and EOF2 in the P1, respectively (Fig. 4a–b). In the P2, the AO-associated CDs were mainly observed over northeastern China and they exhibited moderate and opposite variations over the other parts of

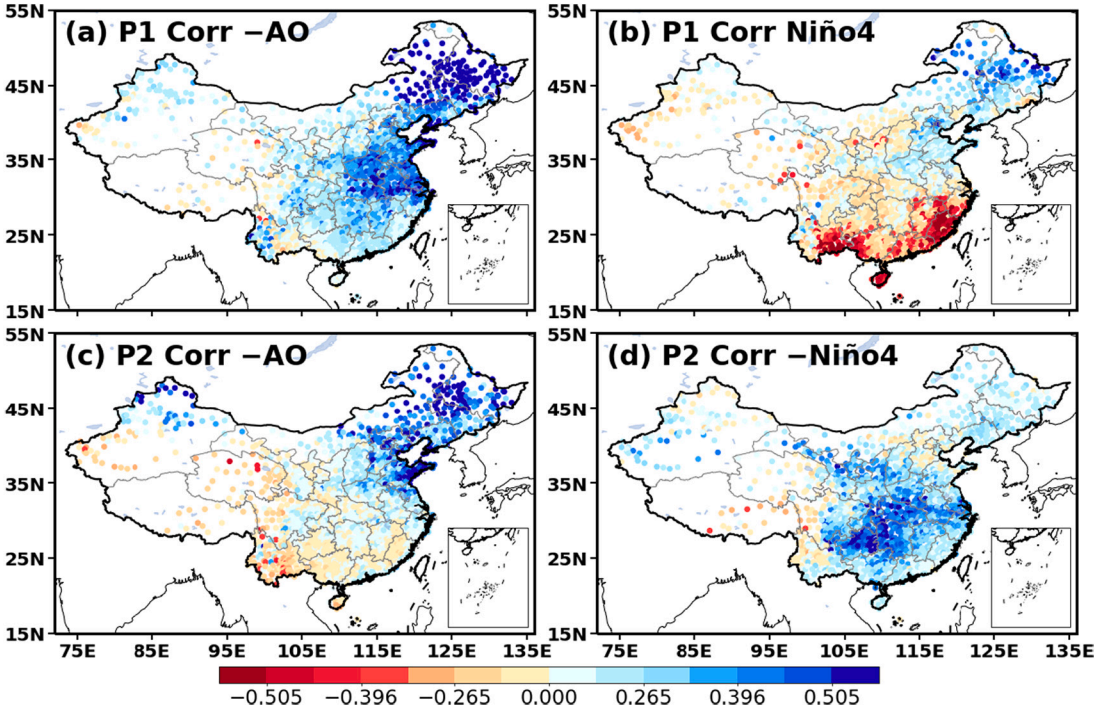

Fig. 7. Correlation maps of CDs with (a) AO index and (b) Niño-4 index in winter during the P1 (detrended). (c–d) Same as in (a–b), but for the P2. Value of 0.396 denotes the significance at the 95% confidence level.

the country, similar to the spatial structure of the EOF2 (Fig. 4d and 7c). In addition, the ENSO-related cold events were found over central-southwestern China, consistent with the spatial structure of the EOF1 (Fig. 4c and 7d). These features indicate that the first mode of extreme cold events over China was significantly related to the AO in the P1 but to ENSO in the P2. In comparison, the second mode showed an opposite relationship with the AO and ENSO in the two periods compared to the first mode.

Fig. 8 presents the regression maps of 200-hPa and 500-hPa geopotential height and winds onto the detrended negative AO index during the P1 and the P2 in winter. As shown in Fig. 8a–b, during the negative phase of the AO, significant anomalous low pressure and a cyclone appeared at middle-upper levels over northern East Asia in the P1. This quasi-barotropic cyclonic circulation was accompanied by anomalous rising motions and hence adiabatic cooling over northeastern China (Fig. 9a). In addition, it induced anomalous northerly and northeasterly winds over eastern China, favoring southward propagation of cold air and occurrence of extreme cold events (Fig. 9a). These features signified a deepening East Asian trough along the East Asian coast, consistent with those associated with the first mode in the P1. The AO showed a weaker magnitude in the P2 (Fig. 3c–d), and the AO-related cyclone anomalies shifted northwestward compared to that in the P1, which might transport cold air from Siberia to northeastern China (Fig. 8b and d). This northwestward shift of cyclone anomalies limited the main effect of the AO on northeastern China during the P2. There were low-level southerly anomalies over southeastern China, consistent with the slightly negative anomalies of the CDs there (Fig. 9b). According to previous studies, the AO could modulate the pathway of the winter cold air mass in East Asia during different periods (Jhun and Lee, 2004; Yang et al., 2020; Liu et al., 2021).

Fig. 10a–b show the regression maps of 850-hPa geopotential height and winds onto the detrended positive and negative Niño-4 index during the P1 and the P2 in winter, respectively. During the P1, El Niño excited an anomalous southwest-northeast elongated anticyclone over the northwestern Pacific, inducing anomalous southerlies along the eastern coast of China and impeding cold air propagation to southern China (Fig. 10a). Negative geopotential height and westerly anomalies emerged from northern China, favoring the occurrence of extreme cold events (Fig. 10a). During the P2, the SST anomalies associated with La Niña tended to be concentrated to the south of 20°N in the western Pacific compared to the P1 (Fig. 10c–d). Correspondingly, cyclone anomalies developed over the South China Sea (Fig. 10b). This anomalous cyclone resulted in anomalous northerly winds (Fig. 10b) and favored cold advection (figures not shown) in the lower troposphere over southern China. The ENSO-related anomalous cyclone shifted westward compared to that in the P1 (Fig. 10a and b), favoring cold air propagation to central-southwestern China and producing an anomalous pattern of CDs similar to the EOF1 in the P2 (Fig. 4c).

6. Summary and discussion

Extreme cold events exert substantial effects on the society, and thus they have received increasing attentions for research in the recent years. In this study, the dominant interannual modes of winter CDs in China and their relationships with the AO and ENSO are investigated, with applications of station observations and global reanalysis datasets.

During the entire period of 1961–2017, the number of climatological winter CDs was evenly distributed over China (about 8–10 days per year), and the national-averaged CDs exhibited a remarkable decreasing trend. The first EOF mode of the CDs reflected a coherent interannual variability with a maximum center over central China, while the second mode represented a north-south dipole variation. These two major EOF modes explained more than half of the interannual variability of China cold events. In addition, the correlation coefficient between the PC1 and CDs averaged over China was 0.996, statistically exceeding the 99.9% confidence level, suggesting that the dominant features of interannual variability of the CDs in China were well reflected by the first mode.

Both the climatological CDs and the dominant modes of the CDs in China displayed an interdecadal shift in the 1980s. The number of winter CDs in China varied from 4 to 24 days during 1961–1985 (P1) to 0–8 days during 1993–2017 (P2), with a weaker interannual oscillation of the national-averaged CDs during the P2 compared to the P1. The first

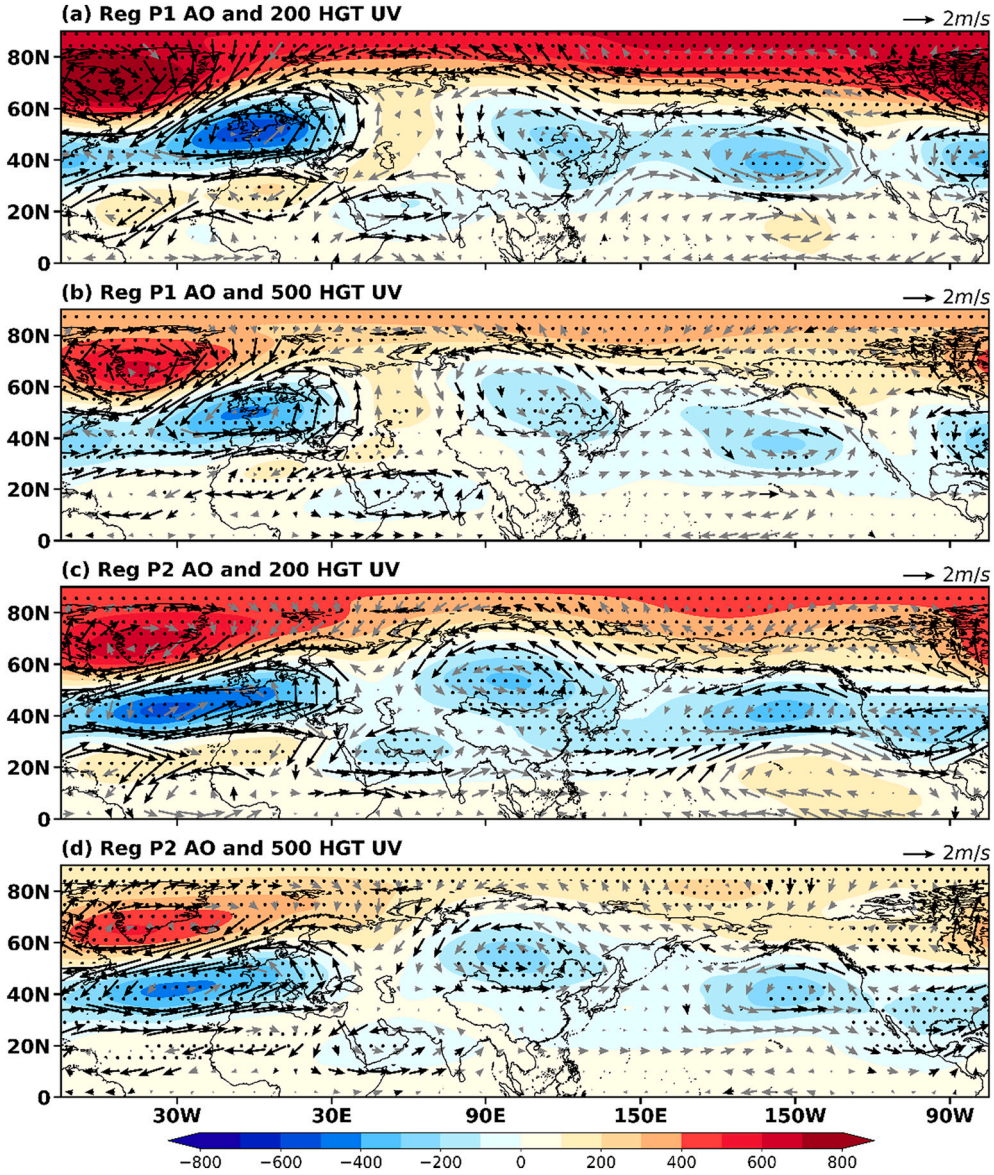

Fig. 8. Regression maps of 200-hPa geopotential height (shading; Pa) and winds (vectors; m s^{-1}) onto the negative AO index in winter (detrended) during the (a) P1 and the (c) P2. (b, d) Same as in (a, c), but for 500-hPa geopotential height and winds. Significant values exceeding the 95% confidence level are marked by black dots or vectors.

mode was depicted by a nearly nationally-coherent structure with a maximum center over central-northeastern China in the P1. However, the maximum center shifted to central-southwestern China and a slightly opposite variation of the CDs appeared over northeastern China in P2. The second mode was characterized by a north-south dipole structure in the two periods, with a maximum center over southern China in the P1 and over northeastern China in P2.

A further analysis suggested that the dominant modes of CDs in China during the two periods was linked to the AO and ENSO. Specifically, the EOF1 was significantly related to the AO in the P1 and ENSO in the P2, whereas the EOF2 was closely connected with ENSO in the P1 and the AO in the P2. During the P1, the negative AO induced an anomalous quasi-barotropic cyclone over northern East Asia, deepening the East Asian trough and hence resulting in anomalous ascending motions and northerlies over central-northeastern China. These atmospheric processes were favorable for the occurrence of CDs over central-northeastern China, producing a spatial structure of CDs similar to the feature associated with the EOF1 in the P1 (Fig. 11a). In the P2, the AO was weaker, and the AO-related cyclone anomalies shifted northwestward (compared to the P1), which was unfavorable for deepening the East Asian trough, limiting its effect to northeastern China and inducing a north-south dipole pattern (Fig. 11b). On the other hand, El Niño excited an anomalous anticyclonic circulation over the Northwest Pacific, impeding cold air thus causing fewer CDs along the coast of southern China, which explained the EOF2 pattern in the P1 (Fig. 11a). Then, in the P2, under a weakening effect of the AO, ENSO played a more dominant role in modulating the first mode. The SST anomalies associated with La Niña events mainly appeared to the south of 20°N in the western Pacific (compared to the P1). These warmer SST anomalies induced a further westward-located and ENSO-related cyclonic circulation that resulted in anomalous northerly wind and cold advection in the lower troposphere over southern China, favoring cold air to propagate to central-southwestern China and producing EOF1-like pattern of the CDs in the P2 (Fig. 11b).

This study emphasizes an interdecadal shift of the roles of the AO and ENSO in modulating the interannual variation of cold events in China. Previous studies have revealed that the Atlantic Multidecadal oscillation (AMO) and the Pacific Decadal Oscillation (PDO) could modulate the

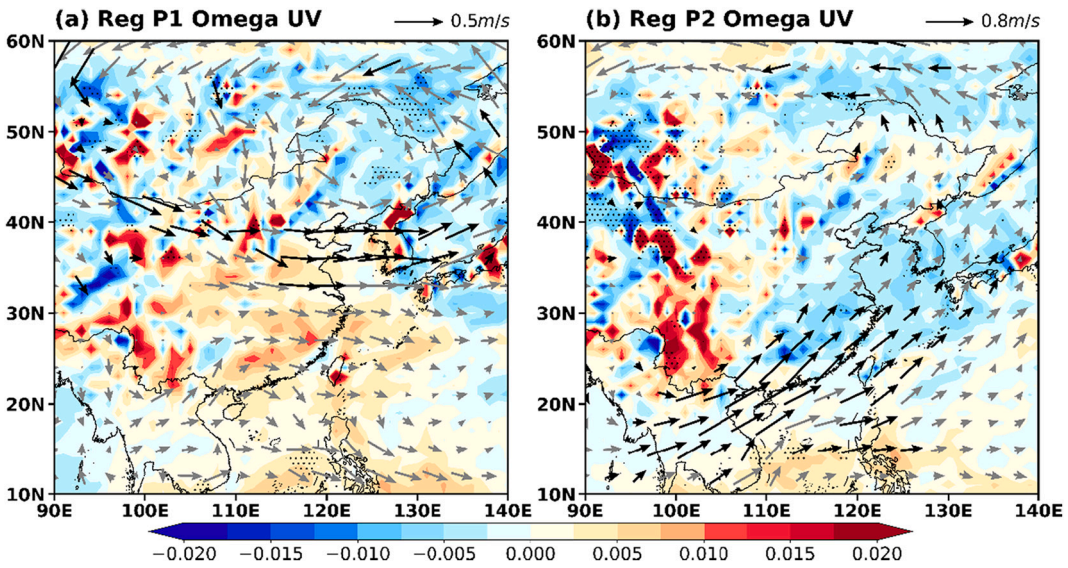

Fig. 9. Regression maps of 500-hPa vertical velocity (shading; Pa s^{-1}) and 850-hPa winds (vectors; m s^{-1}) onto the negative AO index in winter (detrended) during the (a) P1 and the (b) P2. Significant values exceeding the 95% confidence level are marked by black dots or vectors.

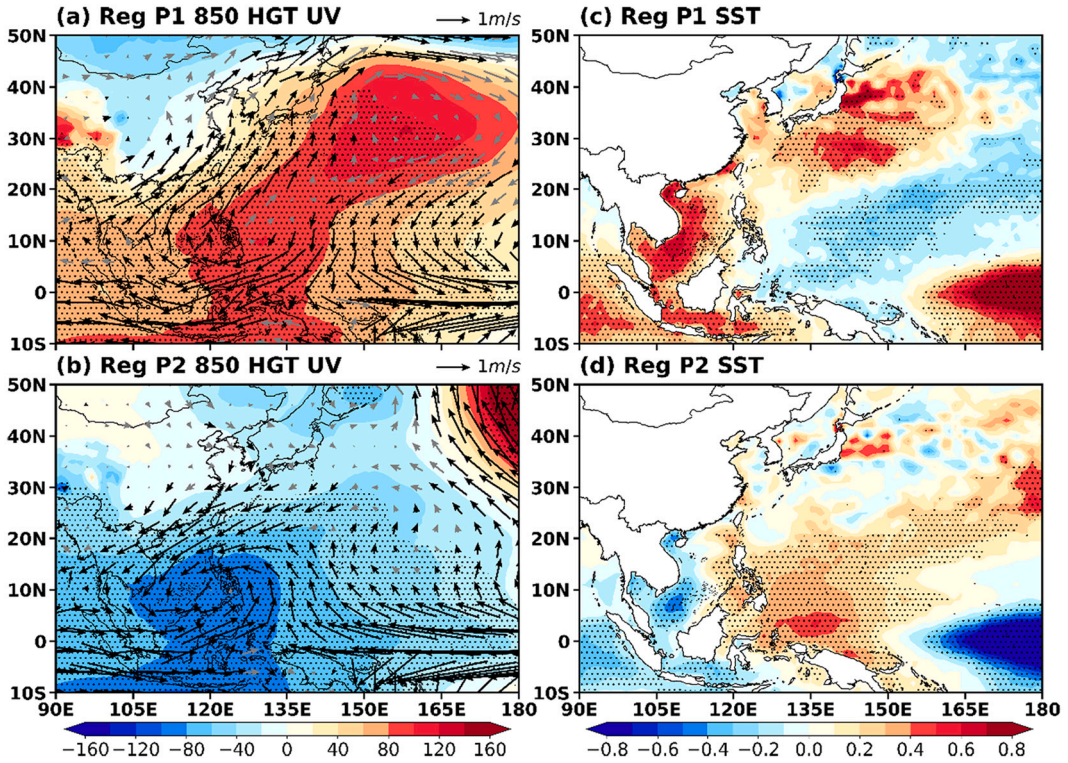

Fig. 10. Regressions of 850-hPa geopotential height (shading; Pa) and winds (vectors; m s^{-1}) onto positive Niño-4 index (a; for the P1) and negative Niño-4 index (b; for the P2) in winter (detrended), respectively. (c–d) Same as in (a–b), but for SST (shading; °C). Significant values exceeding the 95% confidence level are marked by black dots or vectors.

impact of ENSO on the East Asian winter monsoon (Li and Bates, 2007; Wang et al., 2008; He and Wang, 2013), while AMO could also affect China extreme CDs via regulating the Ural blocking (Zuo et al., 2021). Gong et al. (2018) suggested that the AO seemed to be fundamentally rooted in the variability over the North Atlantic and that the structure of the AO could modulate its relationship with regional surface air temperature. In addition, Chen et al. (2013b) revealed the combined effects of the AO and ENSO on the winter climate anomalies in East Asia, although they might be affected by the stratosphere-troposphere interaction and the extratropical-tropical interaction. Moreover, these atmospheric interactions (teleconnections) depend on the background atmospheric circulations as well. Nevertheless, how the interdecadal changes in the mean state, the AMO, and the PDO influence the impacts of the AO and ENSO on cold events warrant further investigations.

CRediT authorship contribution statement

Weiwei Wang: Conceptualization, Methodology, Software,

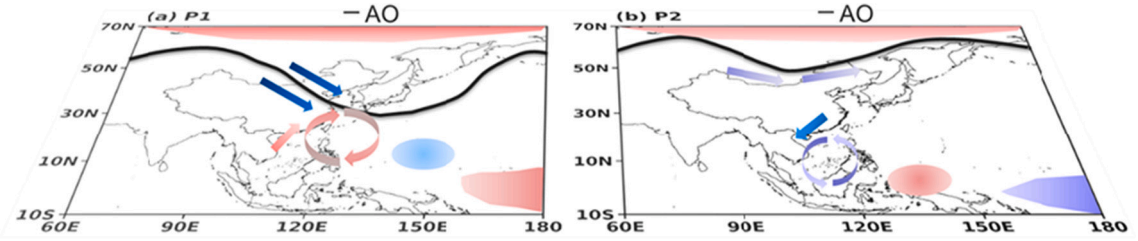

Fig. 11. Schematic diagram showing the mechanism for the interdecadal shift in the relationships of the CDs with the AO and ENSO in the P1 and P2. (a) During the P1, the negative AO was favorable for deepening the East Asian trough along the East Asian coast, resulting in northerlies and hence the southward propagation of cold air and the occurrence of extreme cold events over central-northeastern China (i.e. the first mode in the P1). El Niño excited an anomalous anticyclonic circulation over the Northwest Pacific, accompanied by anomalous southerlies along the east coast of China, impeding cold air and thus causing fewer CDs along the coast of southern China (i.e. the second mode in the P1). (b) During the P2, the AO was weaker, which was unfavorable for deepening the East Asian trough, limiting its effect to northeastern China (i.e. the second mode in the P2). La Niña excited an anomalous cyclonic circulation over the South China Sea, accompanied by anomalous northerly wind, favoring cold air propagation to central-southwestern China (i.e. the first mode in the P2).

Validation, Formal analysis, Writing – original draft, Writing – review & editing. **Song Yang:** Conceptualization, Methodology, Writing – review & editing, Supervision, Funding acquisition. **Qingquan Li:** Investigation, Resources, Funding acquisition. **Tuantuan Zhang:** Conceptualization, Methodology, Formal analysis, Writing – original draft, Writing – review & editing, Supervision, Project administration, Funding acquisition. **Xingwen Jiang:** Investigation, Resources.

Declaration of Competing Interest

The authors declare that they have no known competing financial interests or personal relationships that could have appeared to influence the work reported in this paper.

Data availability

Data will be made available on request.

Acknowledgments

This research was jointly supported by the Guangdong Major Project of Basic and Applied Basic Research (Grant 2020B0301030004), the National Natural Science Foundation of China (Grants 42105015, 41790471, and 42088101), and the Guangdong Province Key Laboratory for Climate Change and Natural Disaster Studies (Grant 2020B1212060025).

References

Bell, B., Hersbach, H., Simmons, A., Berrisford, P., Dahlgren, P., Horányi, A., Muñoz-Sabater, J., Nicolas, J., Radu, R., Schepers, D., Soci, C., Villaume, S., Bidlot, J.R., Haimberger, L., Woollen, J., Buontempo, C., Thépaut, J.N., 2021. The ERA5 global reanalysis: preliminary extension to 1950. Q. J. R. Meteorol. Soc. 147, 4186–4227. https://doi.org/10.1002/qj.4174.

Cao, L., Zhu, Y., Tang, G., Yuan, F., Yan, Z., 2016. Climatic warming in China according to a homogenized data set from 2419 stations. Int. J. Climatol. 36, 4384–4392. https://doi.org/10.1002/joc.4639.

Chen, S., Chen, W., Wei, K., 2013a. Recent trends in winter temperature extremes in eastern China and their relationship with the Arctic Oscillation and ENSO. Adv. Atmos. Sci. 306 (30), 1712–1724. https://doi.org/10.1007/S00376-013-2296-8.

Chen, W., Lan, X.Q., Wang, L., Ma, Y., 2013b. The combined effects of the ENSO and the Arctic Oscillation on the winter climate anomalies in East Asia. Chinese Sci. Bull. 5812 (58), 1355–1362. https://doi.org/10.1007/S11434-012-5654-5.

Cheung, H.N., Zhou, W., Mok, H.Y., Wu, M.C., 2012. Relationship between Ural–Siberian blocking and the East Asian winter monsoon in relation to the Arctic Oscillation and the El Niño–Southern Oscillation. J. Clim. 25, 4242–4257. https://doi.org/10.1175/JCLI-D-11-00225.1.

Cheung, H.H.N., Zhou, W., Lee, S.M., Tong, H.W., 2015. Interannual and interdecadal variability of the number of cold days in Hong Kong and their relationship with large-scale circulation. Mon. Weather Rev. 143, 1438–1454. https://doi.org/10.1175/MWR-D-14-00335.1.

Cui, L., Shi, J., Du, H., Wen, K., 2017. Characteristics and trends of climatic extremes in China during 1959–2014. J. Trop. Meteorol. 23, 368–379. https://doi.org/10.16555/j.1006-8775.2017.04.003.

Curtis, S., Fair, A., Wistow, J., Val, D.V., Oven, K., 2017. Impact of extreme weather events and climate change for health and social care systems. Environ. Heal. A Glob. Access Sci. Source 16, 23–32. https://doi.org/10.1186/S12940-017-0324-3/METRICS.

Dawson, A., 2016. EOFS: a library for EOF analysis of meteorological, oceanographic, and climate data. J. Open Res. Softw. 4, 14. https://doi.org/10.5334/JORS.122.

Deng, K., Yang, S., Ting, M., Zhao, P., Wang, Z., 2019. Dominant modes of China summer heat waves driven by global sea surface temperature and atmospheric internal variability. J. Clim. 32, 3761–3775. https://doi.org/10.1175/JCLI-D-18-0256.1.

Fu, D., Ding, Y., 2021. The study of changing characteristics of the winter temperature and extreme cold events in China over the past six decades. Int. J. Climatol. 41, 2480–2494. https://doi.org/10.1002/joc.6970.

Gao, W., Duan, K., Li, S., 2021. A spatial–temporal analysis of cold surge days in northern China during 1960–2016. Nat. Hazards 108, 147–162. https://doi.org/10.1007/S11069-021-04659-Z/FIGURES/7.

Gong, H., Wang, L., Chen, W., Nath, D., 2018. Multidecadal fluctuation of the wintertime Arctic Oscillation pattern and its implication. J. Clim. 31, 5595–5608. https://doi.org/10.1175/JCLI-D-17-0530.1.

Grotjahn, R., Black, R., Leung, R., Wehner, M.F., Barlow, M., Bosilovich, M., Gershunov, A., Gutowski, W.J., Gyakum, J.R., Katz, R.W., Lee, Y.-Y., Lim, Y.-K., Prabhat, 2015. North American extreme temperature events and related large scale meteorological patterns: a review of statistical methods, dynamics, modeling, and trends. Clim. Dyn. 46, 1151–1184. https://doi.org/10.1007/s00382-015-2638-6.

He, S., Wang, H., 2013. Oscillating relationship between the East Asian winter monsoon and ENSO. J. Clim. 26, 9819–9838. https://doi.org/10.1175/JCLI-D-13-00174.1.

He, S., Gao, Y., Li, F., Wang, H., He, Y., 2017. Impact of Arctic Oscillation on the East Asian climate: a review. Earth-Science Rev. 164, 48–62. https://doi.org/10.1016/J.EARSCIREV.2016.10.014.

Hersbach, H., Bell, B., Berrisford, P., Hirahara, S., Horányi, A., Muñoz-Sabater, J., Nicolas, J., Peubey, C., Radu, R., Schepers, D., Simmons, A., Soci, C., Abdalla, S., Abellan, X., Balsamo, G., Bechtold, P., Biavati, G., Bidlot, J., Bonavita, M., De Chiara, G., Dahlgren, P., Dee, D., Diamantakis, M., Dragani, R., Flemming, J., Forbes, R., Fuentes, M., Geer, A., Haimberger, L., Healy, S., Hogan, R.J., Hólm, E., Janisková, M., Keeley, S., Laloyaux, P., Lopez, P., Lupu, C., Radnoti, G., de Rosnay, P., Rozum, I., Vamborg, F., Villaume, S., Thépaut, J.N., 2020. The ERA5 global reanalysis. Q. J. R. Meteorol. Soc. 146, 1999–2049. https://doi.org/10.1002/qj.3803.

Hu, C., Yang, S., Wu, Q., 2015. An optimal index for measuring the effect of East Asian winter monsoon on China winter temperature. Clim. Dyn. 45, 2571–2589. https://doi.org/10.1007/s00382-015-2493-5.

Jhun, J.G., Lee, E.J., 2004. A new East Asian winter monsoon index and associated characteristics of the winter monsoon. J. Clim. 17, 711–726. https://doi.org/10.1175/1520-0442(2004)017<0711:ANEAWM>2.0.CO;2.

Jian, Y., Leung, M.Y.T., Zhou, W., Jian, M., Yang, S., Lin, X., 2021. Interdecadal shift of the relationship between ENSO and winter synoptic temperature variability over the Asian–Pacific–American region in the 1980s. J. Clim. 34, 5321–5335. https://doi.org/10.1175/JCLI-D-20-0931.1.

Kang, L., Chen, W., Wang, L., Chen, L., 2009. Interdecadal variations of winter temperature in China and their relationship with the atmospheric circulation and sea surface temperature. Clim. Environ. Res. 14, 45–53. https://doi.org/10.3878/j.issn.1006-9585.2009.01.05.

Li, S., Bates, G.T., 2007. Influence of the Atlantic Multidecadal Oscillation on the winter climate of East China. Adv. Atmos. Sci. 24, 126–135. https://doi.org/10.1007/s00376-007-0126-6.

Liu, Y., He, S., Li, F., Wang, H., Zhu, Y., 2017. Interdecadal change between the Arctic Oscillation and East Asian climate during 1900–2015 winters. Int. J. Climatol. 37, 4791–4802. https://doi.org/10.1002/JOC.5123.

Liu, Q., Chen, G., Wang, L., Kanno, Y., Iwasaki, T., 2021. Southward cold airmass flux associated with the East Asian winter monsoon: diversity and impacts. J. Clim. 1–37 https://doi.org/10.1175/jcli-d-20-0319.1.

Lu, C., Zhou, B., 2018. Influences of the 11-yr sunspot cycle and polar vortex oscillation on observed winter temperature variations in China. J. Meteorol. Res. 323 (32), 367–379. https://doi.org/10.1007/S13351-018-7101-2.

Lu, C., Zhou, B., Ding, Y., 2016. Decadal variation of the Northern Hemisphere annular mode and its influence on the East Asian trough. J. Meteorol. Res. 304 (30), 584–597. https://doi.org/10.1007/S13351-016-5105-3.

McMichael, A.J., 2013. Globalization, climate change, and human health. N. Engl. J. Med. 368, 1335–1343. https://doi.org/10.1056/NEJMRA1109341/SUPPL_FILE/NEJMRA1109341_DISCLOSURES.PDF.

North, G.R., Bell, T.L., Cahalan, R.F., Moeng, F.J., 1982. Sampling errors in the estimation of empirical orthogonal functions. Mon. Weather Rev. 110, 699–706.

Om, K.-C., Ren, G., Kim, K.-H., Pak, Y.-I., Jong, S.-I., Kil, H.-N., 2022. Observed trends in extreme temperature events over northern part of the Korean Peninsula during 1960–2019 and a comparative overview. Atmos. Res. https://doi.org/10.1016/J.ATMOSRES.2022.106061, 106061.

Park, T.W., Ho, C.H., Yang, S., Jeong, J.H., 2010. Influences of Arctic Oscillation and Madden-Julian Oscillation on cold surges and heavy snowfalls over Korea: a case study for the winter of 2009-2010. J. Geophys. Res. Atmos. 115 https://doi.org/10.1029/2010JD014794.

Park, T.W., Ho, C.H., Yang, S., 2011. Relationship between the Arctic Oscillation and cold surges over East Asia. J. Clim. 24, 68–83. https://doi.org/10.1175/2010JCLI3529.1.

Ren, Z., Yu, Y., Zou, F., Xu, Y., 2012. Quality detection of surface historical basic meteorological data. J. Appl. Meteorol. Sci. 23, 739–747.

Shang, N., Zhang, X., 2021. Analysis of extreme cold weather event in Texas of February 2021 and suggestions for China. In: The 10th Renewable Power Generation Conference (RPG 2021), pp. 252–257. https://doi.org/10.1049/ICP.2021.2213.

Shi, J., Cui, L., Ma, Y., Du, H., Wen, K., 2018. Trends in temperature extremes and their association with circulation patterns in China during 1961–2015. Atmos. Res. 212, 259–272. https://doi.org/10.1016/J.ATMOSRES.2018.05.024.

Song, L., Wu, R., 2017. Processes for occurrence of strong cold events over Eastern China. J. Clim. 30, 9247–9266. https://doi.org/10.1175/JCLI-D-16-0857.1.

Song, S., Yan, X., 2021. Changes in the frequency of extreme cooling events in winter over China and their relationship with Arctic Oscillation. Sustain. 13 https://doi.org/10.3390/su132011491.

Wang, L., Chen, W., 2010. Downward Arctic Oscillation signal associated with moderate weak stratospheric polar vortex and the cold December 2009. Geophys. Res. Lett. 37 https://doi.org/10.1029/2010GL042659.

Wang, L., Chen, W., 2013. The East Asian winter monsoon: re-amplification in the mid-2000s. Chin. Sci. Bull. 59, 430–436. https://doi.org/10.1007/s11434-013-0029-0.

Wang, L., Lu, M.-M., 2017. The East Asian winter monsoon. In: The Global Monsoon System, pp. 51–61. https://doi.org/10.1142/9789813200913_0005.

Wang, L., Chen, W., Huang, R., 2008. Interdecadal modulation of PDO on the impact of ENSO on the east Asian winter monsoon. Geophys. Res. Lett. 35, 20702. https://doi.org/10.1029/2008GL035287.

Wang, L., Chen, W., Zhou, W., Huang, R., 2009. Interannual variations of East Asian trough axis at 500 hPa and its association with the East Asian winter monsoon pathway. J. Clim. 22, 600–614. https://doi.org/10.1175/2008JCLI2295.1.

Wang, Z., Ding, Y., Zhou, B., Chen, L., 2020. Comparison of two severe low-temperature snowstorm and ice freezing events in China: role of Eurasian mid-high latitude circulation patterns. Int. J. Climatol. 40, 3436–3450. https://doi.org/10.1002/JOC.6406.

Wang, L., Zheng, C., Liu, Y., 2021. Understanding the East Asian winter monsoon in 2018 from the intraseasonal perspective. Clim. Dyn. 57, 2053–2062. https://doi.org/10.1007/S00382-021-05793-X/FIGURES/7.

Wen, M., Yang, S., Kumar, A., Zhang, P., 2009. An analysis of the large-scale climate anomalies associated with the snowstorms affecting China in January 2008. Mon. Weather Rev. 137, 1111–1131. https://doi.org/10.1175/2008MWR2638.1.

Xiao, D., Zuo, Z., Zhang, R., Zhang, X., He, Q., 2018. Year-to-year variability of surface air temperature over China in winter. Int. J. Climatol. 38, 1692–1705. https://doi.org/10.1002/joc.5289.

Yang, H., Fan, K., 2022. Reversal of monthly East Asian winter air temperature in 2020/21 and its predictability. Atmos. Ocean. Sci. Lett. 15 https://doi.org/10.1016/J.AOSL.2021.100142, 100142.

Yang, X., Zeng, G., Zhang, G., Li, Z., 2020. Interdecadal variation of winter cold surge path in East Asia and its relationship with arctic sea ice. J. Clim. 33, 4907–4925. https://doi.org/10.1175/JCLI-D-19-0751.1.

Yun, K.S., Seo, Y.W., Ha, K.J., Lee, J.Y., Kajikawa, Y., 2014. Interdecadal changes in the Asian winter monsoon variability and its relationship with ENSO and AO. Asia-Pacific J. Atmos. Sci. 504 (50), 531–540. https://doi.org/10.1007/S13143-014-0042-5.

Zhang, X., Fu, Y., Han, Z., Overland, J.E., Rinke, A., Tang, H., Vihma, T., Wang, M., 2021. Extreme cold events from East Asia to North America in winter 2020/21: comparisons, causes, and future implications. Adv. Atmos. Sci. 2021, 1–13. https://doi.org/10.1007/S00376-021-1229-1.

Zhang, T., Tam, C.Y., Lau, N.C., Wang, J., Yang, S., Chen, J., Yu, W., Jiang, X., Gao, P., 2022. Influences of the boreal winter Arctic Oscillation on the peak-summer compound heat waves over the Yangtze–Huaihe river basin: the North Atlantic capacitor effect. Clim. Dyn. 1, 1–13. https://doi.org/10.1007/S00382-022-06212-5/FIGURES/12.

Zhao, N., Chen, M., 2021. A comprehensive study of spatiotemporal variations in temperature extremes across China during 1960-2018. Sustain. 13, 3807. https://doi.org/10.3390/su13073807.

Zheng, F., Yuan, Y., Ding, Y., Li, K., Fang, X., Zhao, Y., Sun, Y., Zhu, J., Ke, Z., Wang, J., Jia, X., 2021. The 2020/21 extremely cold winter in China influenced by the synergistic effect of La Niña and warm Arctic. Adv. Atmos. Sci. https://doi.org/10.1007/s00376-021-1033-y.

Zhou, W., Chan, J.C.L., Chen, W., Ling, J., Pinto, J.G., Shao, Y., 2009. Synoptic-scale controls of persistent low temperature and icy weather over Southern China in January 2008. Mon. Weather Rev. 137, 3978–3991. https://doi.org/10.1175/2009MWR2952.1.

Zhou, B., Xu, Y., Wu, J., Dong, S., Shi, Y., 2016. Changes in temperature and precipitation extreme indices over China: analysis of a high-resolution grid dataset. Int. J. Climatol. 36, 1051–1066. https://doi.org/10.1002/JOC.4400.

Zuo, Z., Li, M., An, N., Xiao, D., 2021. Variations of widespread extreme cold and warm days in winter over China and their possible causes. Sci. China Earth Sci. https://doi.org/10.1007/s11430-021-9836-0.